Band gap bowing and spectral width of $Ga_{(1-x)}In_xN$ alloys for modelling Light Emitting Diodes

Christian Tantardini*,†,‡ and Xavier Gonze*,†,¶

†*Skolkovo Institute of Science and Technology, Skolkovo Innovation Center, Nobel St. 3, Moscow, 143026, Russian Federation.*

‡*Institute of Solid State Chemistry and Mechanochemistry SB RAS, 630128 Novosibirsk, Russian Federation.*

¶*European Theoretical Spectroscopy Facility, Institute of Condensed Matter and Nanosciences, Université catholique de Louvain, Chemin des étoiles 8, bte L07.03.01, B-1348 Louvain-la-Neuve, Belgium*

E-mail: christiantantardini@ymail.com; xavier.gonze@uclouvain.be;X.Gonze@skoltech.ru

Abstract

$Ga_{(1-x)}In_xN$ alloys, widely employed to produce light-emitting diodes, exhibit a bowing of the band gap as a function of concentration x, and a luminescence spectral width which differs from the expected value of 1.8 kT. Through first-principles calculations, based on many-body perturbation theory and density-functional theory with a meta-GGA exchange-correlation functional, we explore jointly these effects, in an exhaustive set of $Ga_{(1-x)}In_xN$ supercells with 16 atoms. We disentangle the bowing due to the average volume change with the one due local atomic configuration and local relaxation. The first one account for about 40% of the bowing, despite that fact that the change of volume with respect to concentration is nearly linear (Vegard's law).

The computed bowing parameter is 1.39 eV. The experimental broadening between 3kT and 8kT, not examined theoretically until now, is well accounted by local atomic configuration changes and lifting of the degeneracy of the top of the valence band.

Introduction

Light-emitting diodes (LEDs) are used in devices where brightness, low power consumption, and reliability are sought, such as automotive, mobile and display applications. Most bright LEDs are based on group-III nitride semiconductors or their alloys, $Al_xGa_yIn_{(1-x-y)}N$, which can emit efficiently in the near ultraviolet, violet, blue, cyan, and green wavelength range. Combined with phosphors, nitride-based devices can generate white light with coverage of the whole visible spectrum. Although nitrides are important to make LEDs, their synthesis is complicated, so that in most of the cases the quality of samples is not good enough to accurately measure altogether lattice parameters[1–5], fundamental band gap[5–8] and splitting energies of bands[5,9–11]. This makes difficult to study the dependence of band gap on the concentration of group-III elements within such nitrides. In addition, in group-III nitrides alloys, the average band gap does not vary linearly with the concentration, but a pronounced *bowing behavior* is observed[12,13].

Such bowing is observed for wurtzite structures of $Ga_{(1-x)}In_xN$ alloys, on which we focus in the present study, with spectral range from ultraviolet for pure GaN to red for pure InN[3,14–31]. In ternary (and quaternary) III–V alloy semiconductors, one observes an emission linewidth in the range between 3 and 8 kT, that is about 0.08 to 0.2 eV[32,33], broader than the theoretical expected value due to thermal fluctuations, namely 1.8 kT[32–36]. It has been hypothetized that *alloy broadening* (*i.e.*, the statistical fluctuation of the active region alloy composition) determine such spectral width at room temperature, but such hypothesis has not been theoretically confirmed to our knowledge. The atomic substitution of Ga by In inside wurtzite structures does not deliver preferred orderings or segregations at specific concentrations. With such absence of intermediate phases, the band gap is a smooth and

continuous function of concentration, albeit with the above-mentioned broadened spectral emission.

In binary alloys, like $Ga_{(1-x)}In_xN$, the bowing parameter, b, is traditionally defined as the coefficient of the non-linear term in the phenomenological expression

$$E_g(x) = xE_g^{InN} + (1-x)E_g^{GaN} - bx(1-x), \tag{1}$$

where E_g^{InN} is the energy band for the pure wurtzite InN and E_g^{GaN} for the pure wurtzite GaN. A positive b parameter indicates smaller energy gap than the linear combination of end-point band gaps. Generalized bowing parameters can be defined for quaternary alloys. To design LEDs with specific optical confinement, the knowledge of bowing parameter(s) is of fundamental importance.

For $Ga_{(1-x)}In_xN$, different values of b have been observed for samples with different concentrations of x, and experimental and theoretical data also do not agree with each others[3,12–29,37–41]. This of course raises questions about the adequacy of Eq. 1. More insights in the behavior of band gap bowing in $Ga_{(1-x)}In_xN$ alloys, possibly beyond the dependence upon the single parameter x, might allow to better control the band gap and its relation with the stress, with easier control of emission wavelength inhomogeneities in the production of large wafers for LEDs.

The study of deviation of band gap linearity from GaN to InN in $Ga_{(1-x)}In_xN$ alloys is hampered by inaccuracies of band gap estimation. While accurate measurements of GaN wurtzite band gap were performed many years ago[18–29,38,42] delivering E_g^{GaN} 3.50 eV, the band gap in pure InN wurtzite is still debated, being estimated in the range from E_g^{InN}=0.7 to 2.0 eV[18–29,38–40,43]. Band gap measurements for InN wurtzite are affected by Burstein-Moss shift and non-parabolic conduction band[21]. The different growth techniques employed are seen to affect the estimation of band gap in pure InN wurtzite structure and in In-rich $Ga_{(1-x)}In_xN$ alloys. Although for these alloys different band gap values are estimated, the

band gap bowing is seen to be small (*i.e.*, b 1.4 eV) for $0.5 \leq x \leq 1.0$[22]. A small bowing band gap (*e.i.*, b=1.0 eV) was also initially observed for $Ga_{(1-x)}In_xN$ alloys Ga-rich[44], but was subsequently challenged by other experiments[16,17,26,28]. These experiments showed a large bowing band gap that differs for strained (*i.e.*, b=3.2 to 3.8 eV[16,17,26,28]) and unstrained structures (*i.e.*, $b \approx 2.6$ eV[16,17,28]).

Theoretical works estimating the bowing parameter b through DFT showed strongly dependence by In concentration: b equal to 4.8, 3.5, and 3.0 eV respectively for x =0.0625, 0.125 and 0.25[16]. The same large bowing at low In concentration was estimated through semi-empirical calculations[15]. The same semi-empirical calculations were performed also at high In concentration ($x \geq 0.6$) showing band gap dependence in presence or absence of strain: higher band gap for the unstrained situation than the strained one[15]. LDA calculations[16,45] were seen to underestimate the band gap, and a better agreement with experimental results was obtained with LDA-1/2 approach[46]. However, such underestimation of the band gap leaves the estimation of the bowing practically unaffected[46]. More accurate calculations were performed with HSE hybrid exchange-correlation DFT functional[47] on $Ga_{(1-x)}In_xN$ wurtzite supercells, however focusing on the analysis of an average band gap, which takes into account the breaking of symmetry due to atomic substitution[48,49]. Such average band gap was estimated for selected $Ga_{(1-x)}In_xN$ wurtzite 16 and 32 atom supercells as the difference between the conduction-band minima and the average of last three valence-band maxima at Γ point[48,49]. The bowing parameter calculated from the average band gap was equal to b=1.10 eV[49], that it is similar to the estimation of Nakamura[44], but lower than the one seen by other experiments[16,17,22,26,28]. More recently, the bowing parameter was estimated equal to b=2.0 eV by HSE calculations, which was seen to be coherent with calculations performed with the G_0W_0 approximation[50]. Furthermore, for such alloys, through HSE calculations the chemical ordering was found having a non-negligible effect on band gap and bowing parameter (*i.e.*, b=0.78 eV for ordered and b=1.35 eV for disordered)[14].

In the present analysis, we will disentangle different effects causing the band gap non-

linear behaviour. Indeed, alloy concentration changes produce a very strong, but *linear* volume variation, the well-known Vegard's law. At constant concentration but varying volume, what is the behaviour of the band gap ? Does it have a non-linear behaviour, and is it quadratic as hypothesized by Eq. 1 ? Alternatively, at constant volume but varying concentration, can we analyze the band gap non-linearities ? The disorder plays a role in the broadening of the emission, and we will pay attention to its role as well. We distinguish thus the subsequent non-linearities of the band gap due to volume change from those due to average concentration changes, and those due to local atomic disorder.

In order to tackle such questions, we will study all possible models for 16-atom per cell wurtzite structures of $Ga_{(1-x)}In_xN$ alloys of varying In concentration, consider different volumes for the same concentrations, and will quantity the alloy broadening in this set of models. The band gap in such structures will be scrutinized using TB09 DFT calculations, whose validity will be established by comparison with G_0W_0 results for smaller cells, as we now explain.

The shortcomings of density-functional theory calculations of gaps based on (semi-)local exchange-correlation functionals (local-density approximation, LDA, or generalized-gradient approximations, GGA), as in most previous studies, are well known[51]. The GW approximation[51,52] is a more reliable approach to the computation of band gaps. However, it is much more computationally demanding than semi-local DFT calculations, even in its non-selfconsistent version G_0W_0. The latter has a dependence on its starting wavefunctions, for example the standard GGA-PBE[53] ones. For InN, this constitutes a serious problem, as the InN gap closes with LDA or GGA, which makes it an inadequate starting point for a G_0W_0 calculation. Non-selfconsistent G_0W_0 methodology based on LDA or GGA exhibits a tendency to underestimate the band gaps anyhow[54]. However, the gaps from G_0W_0 with starting PBE wavefunctions, noted G_0W_0@PBE, still describes the experimental gap more accurately than a systematic linear correction applied on DFT data (e.g. using the GGA-PBE exchange-correlation functional)[53,55].

Instead of LDA or GGA, the DFT electronic band structure can more effectively be computed using the meta-GGA Tran-Blaha (TB09) approach[56]. The TB09 band gap is much more reliable than LDA or GGA ones, and comes at a much lower computational cost than G_0W_0@PBE. Furthermore, one can choose TB09 to provide a better starting point than PBE for G_0W_0 calculations, giving the G_0W_0@TB09 methodology. G_0W_0@TB09 band gaps agree even more with the experimental one than G_0W_0@PBE band gaps, and fixes TB09 issues for bandwidths[57].

While self-consistent quasi-particle GW calculations with electron-hole corrections[54] represent the state of the art in band gap computation at fixed atomic positions, they come with a much higher computational cost than non-self-consistent G_0W_0 calculations. We will not perform such self-consistent calculations, partly because anyhow the remaining discrepancy between such band gap and experimental ones is largely due to zero point renormalization of the band structure from electron-phonon coupling.[58,59] Such coupling gives a correction to the band gap of GaN at zero temperature on the order of 0.2 eV[60]. So, in order to investigate the bowing effect, we will rely mostly on TB09, validated with G_0W_0@TB09 reference calculations for small cells, and ignore further quasi-particle and zero-point renormalization effects. We think that such an approach capture most non-linearities of the band gap dependence on concentration already.

In the present work we will first analyze the consistence between bowing parameter calculated with TB09 and G_0W_0@TB09. This will be done on several models generated by variation of In concentration in $Ga_{(1-x)}In_xN$ alloys. As the results are consistent, we will generate all possible models for 16-atom per cell wurtzite structures of $Ga_{(1-x)}In_xN$ alloys of varying In concentration. Such structures will be optimized with GGA-PBE[53] and their band gaps will be subsequently evaluated with TB09[56]. This will be done in order to provide an accurate estimation of the electronic band gap and subsequently focus our work on the origin of bowing parameter and the associated thermal and alloy broadenings, to understand the modelling of LEDs.

Method and Computational Details

All $Ga_{(1-x)}In_xN$ alloys share an average wurtzite structure, with the cation site occupied by Ga or In. To model such alloys, several arrangements of atoms in (super)cells of $Ga_{1-x}In_xN$, of moderate sizes, are considered. We do not rely on large supercells with random atomic positions, neither on quasi-random structures, as our goal is to disentangle the influences on the band gap from lattice parameters, the chemical site occupation, and the local distortions of the local environment, which can most easily been done by using more regular structures.

The z coordinate being defined along the trigonal axis,we investigate all non-equivalent atomic arrangements of atoms inside 2×2×1 16-atom supercells, albeit avoiding treating in such cells the atomic arrangements that are equivalent to atomic arrangements with smaller cells, respectively 1×1×1 and 2×1×1, with respectively four and eight atoms. We have also explored 1×1×2 and $\sqrt{3} \times \sqrt{3} \times 1$ supercells, with eight and twelve atoms, as reported in the supplementary information, but have decided to focus in the main text on the 16-atom supercell results, already sufficiently instructive and complete. This gives three distinct atomic arrangements in the 1×1×1 (primitive) cell (Ga_2N_2, In_2N_2 and $GaInN_2$), three more distinct atomic arrangements in the 2×1×1 supercell, and 13 more arrangements in the 2×2×1 supercell. The latter presents actually 19 different atomic arrangements, including those that reduce to smaller cells atomic arrangements. We also consider a large 96-atom supercell ($Ga_{47}InN_{48}$) corresponding to a $2\sqrt{3} \times 2\sqrt{3} \times 2$ enlargement of the GaN primitive cell, with one substitution of a Ga atom by an In atom. The different nonequivalent arrangements of atoms in the 2×2×1 supercell span 9 compositions: one arrangement yields GaN; one yields $Ga_{(0.875)}In_{(0.125)}N$; two yield $Ga_{(0.75)}In_{(0.25)}N$, three yield $Ga_{(0.625)}In_{(0.375)}N$; five yield $Ga_{(0.5)}In_{(0.5)}N$; three yield $Ga_{(0.375)}In_{(0.625)}N$; two yield $Ga_{(0.25)}In_{(0.75)}N$; one yields $Ga_{(0.125)}In_{(0.875)}N$; and one yields InN. Some of these atomic arrangements are visualized using the VESTA software[61] in Fig. 1.

All above-mentioned structures are fully optimized with PBE exchange-correlation density functional[53]. The computation of electronic band gap in such optimized geometries, but

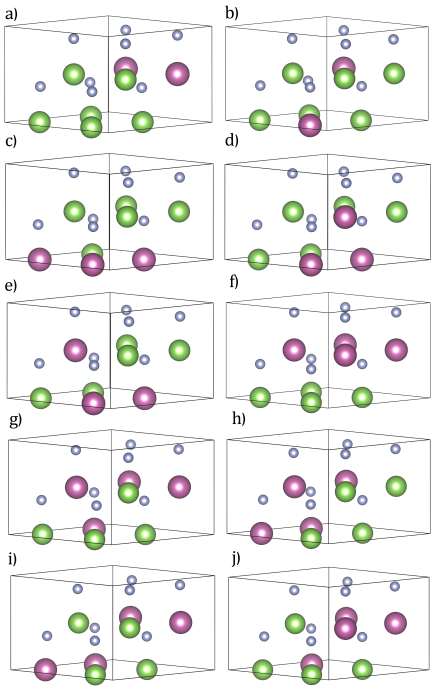

Figure 1: Crystal structures of 16-atom $2 \times 2 \times 1$ $Ga_{(1-x)}In_xN$ supercells: (a and b) $Ga_{(0.75)}In_{(0.25)}N$, (c, d and e) $Ga_{(0.625)}In_{(0.375)}N$, (f, g, h, i and j) $Ga_{(0.5)}In_{(0.5)}N$. Legend: In, pink; Ga, green; N, grey.

also for some other frozen-atom atomic positions (see later) is performed with the TB09[56] exchange-correlation functional, but also (see the supplementary information) with the PBE density functional for reference. The non-self-consistent G_0W_0 calculations are then performed starting from TB09 wavefunctions, yielding G_0W_0@TB09 results, and also, reported in the supplementary information, from PBE wavefunctions, yielding G_0W_0@PBE results.

The geometry optimization relies on Broyden-Fletcher-Goldfarb-Shanno (BFGS) algorithm[62–65], with force tolerance for the maximum net force on atoms fixed at 10^{-6} Ha/bohr. The Γ-centered k-point meshes are: $8 \times 8 \times 8$ for the primitive cell; $4 \times 8 \times 8$ for the $2 \times 1 \times 1$ supercell; $8 \times 8 \times 4$ for the $1 \times 1 \times 2$ supercell; $4 \times 4 \times 8$ for $\sqrt{3} \times \sqrt{3} \times 1$ and $2 \times 2 \times 1$ supercells. For the 96-atom cell, the sampling was based on the Γ point only. Different pseudopotentials were considered: projector augmented-wave (PAW) pseudo-potentials[66] for geometry optimization, with 13 valence electrons for Ga and In and 5 valence electrons for N, and norm-conserving relativistic separable dual-space Gaussian pseudo-potentials[67] with 3 va-

lence electrons for Ga and In and 5 valence electrons for N, for electronic structure band gap calculations (G_0W_0 or TB09), avoiding the use of PAW for GW calculations, following the criticism from Klimes and coworkers.[68] The kinetic energy cutoff is 25 Ha. For G_0W_0 calculations, the number of unoccupied bands per atom is 50 and the energy cut-off for the dielectric matrix is 5 Ha. Only the 4-atom and 8-atom cells were considered in such calculations, as a reliable correlation between TB09 and G_0W_0 results was established, see next section.

In order to separate the effect of the atomic volume from the other effects, we also studied the band gap in the 19 atomic arrangements of the $2 \times 2 \times 1$ supercell with fixed volumes and fixed atomic positions of the GaN crystal, of the InN crystal, and of the $Ga_{(0.5)}In_{(0.5)}N$ cell, the latter with the average volume of the five atomic arrangements with $x = 0.5$ in this $2 \times 2 \times 1$ supercell. All calculations are performed with Abinit version 9.1.6[69–71].

Results and Discussion

In wurtzite $Ga_{(1-x)}In_xN$ alloys, the fundamental band gap is always direct and located at Γ. Thus, hereafter only this fundamental band gap needs to be considered. Furthermore, we will consider the average band gap, calculated as the difference between the conduction-band minimum and the average of the highest three valence-band maxima at Γ point[49]. This is done to take into account the breaking of symmetry in the electronic structure due to the local atomic substitutions in our limited size cells. In real samples, the emission/absorption intensity originates from all such states, and its spread will be analyzed later.

Before investigating the bowing parameter, the band gap value in InN wurtzite needs to be discussed. As mentioned in the introduction, there is a strong dependence of the InN band gap on the crystallization technique. One can assume that the band gap of 1.12 eV, experimentally measured for InN growth as freestanding nanowire[38], is the most independent on the substrate. This makes it the most reliable one compared to other experimental

values[18–29,39,40,43]. Thus, our calculations will be validated with respect to this experimental value. In particular, using the PAW approach, we have tested the treatment of $4d$-electrons of In either included in the core or treated as valence, within the primitive cell 1×1×1 (*i.e.*, 4 atoms per cell). A band gap underestimation due to the treatment of d-electrons as core electrons in In is indeed mentioned in literature[37]. It was also reported in literature[37] that the band gap underestimation does not affect the bowing parameter. Our investigation (see in Supporting Information Fig.1 and Fig.2) confirms the band gap underestimation (*i.e.*, 0.94 eV for TB09 and 0.92 eV for G_0W_0@TB09) when $4d$-electrons are treated as core electrons, while in case $4d$-electrons of In are treated as valence electrons, the InN band gap is 1.19 eV for TB09 and 1.39 eV for G_0W_0@TB09, which are close to the experiment (*i.e.*, 1.12 eV)[38]. Moreover, the narrowing of the band gap due to the zero-point renormalization is expected on the order of 0.15-0.2 eV, based on the similarity (and common light anion) with GaN[59]. Thus, while G_0W_0@TB09 might be the best technique available to compute this band gap, the simpler TB09 methodology still gives a decent gap, on the basis of which the investigation of the bowing can be done. A difference of 0.25 eV due to the treatment of In $4d$-electrons is thus observed in case of TB09, changing to 0.34 eV in case of G_0W_0@TB09. We will stick to the treatment of $4d$-electrons of In as valence electrons in what follows. Interestingly, this difference comes directly from the different volume per atom found for the two optimized structures: $1.09{\cdot}10^{-2}$ (Bohr)^3 when In d-electrons are treated as valence electrons and $1.14{\cdot}10^{-2}$ (Bohr)^3 when In d-electrons are treated as core electrons. The explicit treatment of In $4d$-electrons as valence electrons during the optimization lowers the volume per atom, with corresponding change of band gap[37]. This gives a warning on the importance of the volume dependence to clarify the source of bowing in $Ga_{(1-x)}In_xN$ alloys[50].

After having clarified the value of the band gap at the In-rich end, the focus can be shifted on the band gap deviation from linearity of the $Ga_{(1-x)}In_xN$ alloys, expressed as $E_g(x) - (xE_g^{In} + (1-x)E_g^{Ga})$. Taking into account the importance of the lattice parameters, one can disentangle the pure effect of a change of concentration from the indirect effect

connected to a change of atomic volume. For that purpose, the band gap can be written as a function of two arguments: the concentration x and the atomic volume V, giving $E_g(x, V)$. Of course the atomic volume V is a function of the concentration x at zero pressure, $V(x)$. Still the separate examination of the dependence of the band gap on these two variables $E_g(x) = E_g(x, V(x))$, taken as independent, is legitimate, and allows the decomposition of the deviation from the linear behaviour $E_g(x) - (xE_g^{In} + (1-x)E_g^{Ga})$ as coming from a deviation at fixed concentration but varying volume, and a deviation at fixed volume, but varying concentration.

In this spirit, the band gap has been computed for differently scaled $1 \times 1 \times 1$ cells of $Ga_{(1-x)}In_xN$ with $x := \{0, 0.5, 1\}$. The change of band gap due to varying atomic volume, at constant concentration x, being defined as $\Delta E_g(x, V) = E_g(x, V) - E_g(x, V(x)$, the deviation from linearity of the TB09 band gap and G_0W_0@TB09 band gap is then compared. Generically, in forthcoming figures, the deviation from linearity, for which the symbol "δ" is used, is computed by removing the linear contribution connecting both end points, at $x = 0$ and $x = 1$.

Fig. 2 highlights first the linear correlation between the band gap values obtained with TB09 and those obtained with G_0W_0@TB09 when the structures are subject to strain or compression (see the numerical data in SI Tab.2-4). For this task the lattice parameters 1×1×1 $Ga_{(1-x)}In_xN$ cells with $x := \{0, 0.5, 1\}$, have been scaled, imposing the same volume per atom than in the different $Ga_{(1-x)}In_xN$ 2×2×1 supercells (16-atom per cell). The difference of bowing between TB09 and G_0W_0@TB09 is small, although not completely negligible, namely 0.18 eV at x=0.0, 0.14 eV at x=0.5 and 0.10 eV at x=1.0. This is about one order of magnitude smaller than the expected bowing value b. It was also tested for some 8-atom supercells, and confirmed to be on the same order of magnitude, see the supplementary material. Given the large difference in CPU time, such a difference was deemed to be small enough to characterize from TB09 the band gap bowing for all possible model structures generated by different atomic configurations within 2×2×1 $Ga_{(1-x)}In_xN$ supercells.

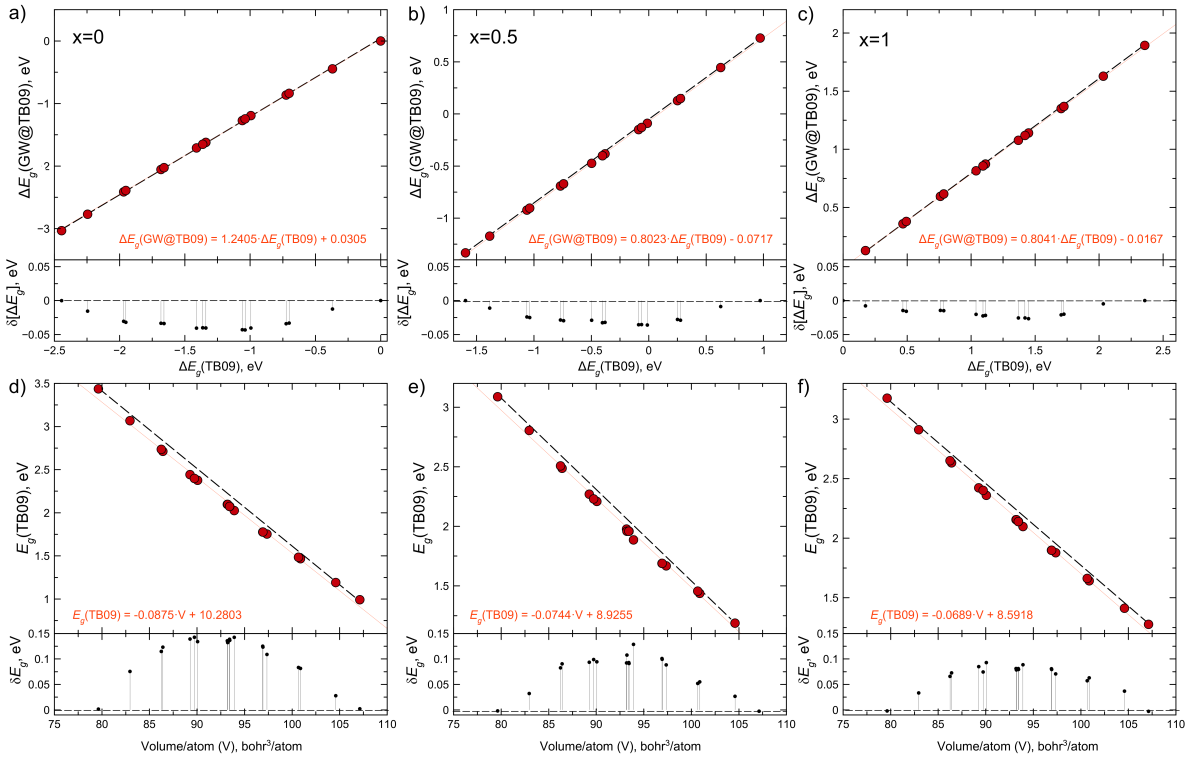

Figure 2: (a-c) Top panels: comparison between change of band gap for varying atomic volumes, at constant concentrations, calculated with TB09 and G_0W_0@TB09. (d-f) Bottom panels: average band gap calculated with TB09 as a function of the atomic volume. Adjacent panels below the top and bottom panels: deviations with respect to perfect linear fit, highlighting their smallness, although a small bowing is present. The systems considered are $Ga_{(1-x)}In_xN$ with $x := \{0, 0.5, 1\}$ (left, middle, right) 1×1×1 cells (4-atom per cell) with different volume per atom corresponding to optimized $Ga_{(1-x)}In_xN$ $2 \times 2 \times 1$ supercells (16-atom per cell) of different concentrations.

Fig. 2d-f shows the dependence of the TB09 band gap on the atomic volume. The linear dominance is obvious, but the quadratic deviation from it can be quantified: the bowing due to this single factor is 0.6 eV at x=0.0, about 0.5 eV at x=0.5 and 0.4 eV at x=1.0. Without even modifying the composition, a bowing is present, simply due to the cell volume change. The increase of strain increases the cell volume, the atomic volume, and gives a bowing of the band gap.

However, in addition to this bowing, there might also be a non-linear change of the atomic volume as a function of the concentration. Typically, in most alloys, a linear behaviour of the atomic volume with the concentration is however observed (Vegard's law). Only very

small deviation from quadraticity are present.

In Fig. 3, the specific effect of varying the concentration x is shown. In the right panel, Fig. 3a, the volume per atom as a function of concentration x in the nineteen 16-atom supercells is represented. The increase of In concentration with consequent reduction of Ga concentration for a stoichiometric compound causes a near linear change in atomic volume. This translates immediately to a modification of the band gap, according to the previous analysis, Fig. 2, but the deviation from the Vegard law is very small, and not obviously quadratic.

Still, the atomic positions for different configurations at constant concentration x can also affect directly the band gap, which is the next possible reason for the bowing. Fig. 3b-d illustrates the band gap variation with concentration x for fixed unit cell and atomic positions (see the SI Tab. 13 to Tab.26) but different configurations even for the same stoechiometry. The range of variation of the band gap from x=0 to x=1 is considerably smaller than the one without volume constraint. One observes globally a small linear trend, whose slope changes with the Ga/In stoechiometry, being nearly negligible for the $Ga_{0.5}In_{0.5}N$ alloy. A widening of the band gap values at constant x, is also present, with pronounced significant lowering with respect to the linear behaviour, which induces, on average, a bowing. For $Ga_{0.5}In_{0.5}N$, we selected one of the five configurations, and fixed its atomic volume to the average of these five, then we performed the replacements with different atomic stoechiometries, but not at x=0.5 (which would be weird). This explains the single point at x=0.5.

So, as the atomic displacement and the concentration x affect together the atomic volume, and consequently the band gap, we expect that they also affect the band gap bowing. Thus, coming to the full story, we have calculated with TB09 the b for all possible relaxed geometric configuration within 16-atom $Ga_{(1-x)}In_{(x)}N$ supercells, see Fig. 4, estimated the parameter b at each concentration x and reported it in the SI Tab.9-12.

As we see in Fig. 4, despite the considerable spread of values, the band gap deviation from linearity can be approximated by a parabolic function with an average b equal to 1.39 eV.

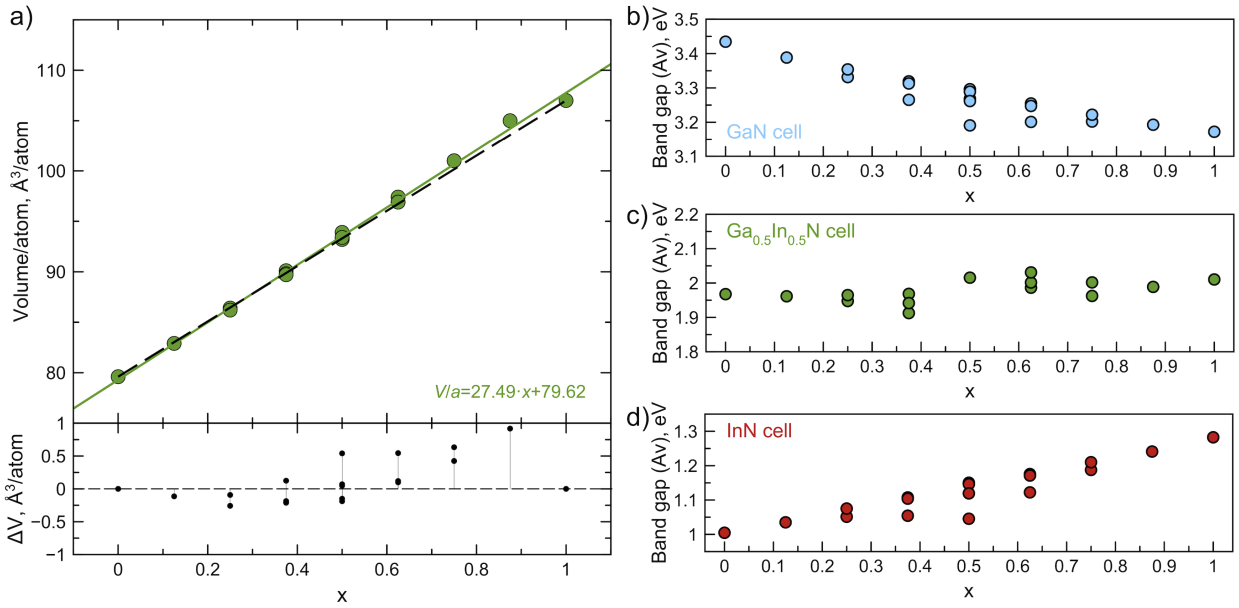

Figure 3: (a) Volume per atom as a function of x calculated by optimization with PBE of wurtzite $2 \times 2 \times 1$ supercells of $Ga_{(1-x)}In_xN$ alloys. In the graph the interpolation line (green) and the straight line (dash black line) from $x = 0$ to $x = 1$ are shown. (b-d) Average band gap calculated with TB09 as a function of concentration x for fixed $2 \times 2 \times 1$ supercells of GaN (cyan), $Ga_{0.5}In_{0.5}N$ (green) and InN (red). The $Ga_{0.5}In_{0.5}N$ volume was fixed to the average volume found for the five structures of that stoechiometry present in the Fig. 1. There was no geometry relaxation in these calculations, only substitution of atoms by others.

It is in agreement with the most recent theoretical value performed with HSE of 1.35 eV[14] and close to experimental value for free standing nanowires of 1.10 eV[38]. According to the previously mentioned analysis, about 40% of the bowing comes from the change of atomic volume, and the remaining from chemical ordering and local relaxations. The considerable spread of the values depending on the specific atomic arrangement at fixed concentration contributes of course to the spectral width observed experimentally, together with the above-mentioned splitting of the top of the valence band. None of the previous studies[3,14–29,37–40] considered all possible structures at different concentration from x=0 to x=1 as we have performed.

Some previous works also showed an increase of bowing parameter with decreasing In concentration[3,14–29,37–40]. However, in our case such an effect does not appear straight in Fig. 4 for which the deviation of band gap linearity is maximum at x=0.5 and decreases

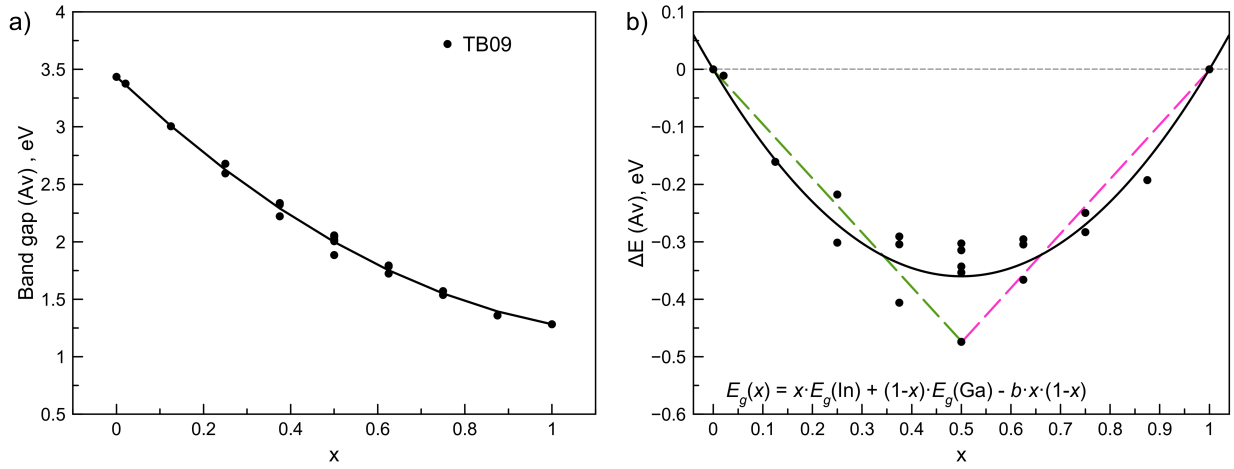

Figure 4: (a) Calculated TB09 band gap as a function of concentration x in $Ga_{(1-x)}In_xN$ 2×2×1 supercells. Values at different concentration x are interpolated by the parabolic function $E_g(x) = xE_g^{In} + (1-x)E_g^{Ga} - bx(1-x)$, with bowing parameter b equal to 1.39 eV. (b) TB09 band gap deviation from linearity $\Delta E = E_g(x) - (xE_g^{In} + (1-x)E^{Ga})$ as a function of concentration x in $Ga_{(1-x)}In_xN$ 2×2×1 supercells. The black line is the term $-bx(1-x)$ with b equal to 1.39 eV. The green dashed line is the straight line between x=0.0 and the lowest x=0.5, while the pink dash line is the straight line between the lowest x=0.5 and x=1.0.

roughly symmetrically with x variation. The computation of the TB09 band gap for a 96-atom supercell with one In atom (so, x=1/48) does not bring evidence for a larger b value at small x. On the contrary, the corresponding point in Fig. 4 appears slightly above the 1.39 eV bowing fit and even above the straight line connecting the x=0 and lowest x=0.5 value shown in Fig. 4b. However, the spread of values appears slightly bigger in the Ga-rich side of the concentration range.

As mentioned in the introduction, in III–V nitride LEDs the expected spectral width for thermally broadened emission is equal to 1.8kT, but is between 3kT and 8kT at room temperature experimentally[32–36]. The increase of spectral width could originate from alloy broadening, that is, statistical fluctuation of the active region alloy composition and local geometries. Within our set of supercells, we can quantify two effects related to the presence of local geometry modifications. The first effect is the existence of a splitting of the three-fold degeneracy of the valence band, while the second effect comes from variations of local atomic configurations at constant concentration. Then, of course there might be concentra-

tion changes with a slower spatial variation than permitted in the 16-atom supercell case. Focusing on the two first effects, three different measures of broadening have been computed. In the first measure, denoted σ_a where a stands for average, we have first averaged the three upper valence bands to determine the average band gap for one particular supercell, then, for the group of supercells with a common concentration, the average of band gaps and their root-mean square deviation σ_a have been computed. In the second measure, denoted σ_s where s stands for split, the three band gaps have been considered separately, for each supercell, then a global computation of the band gap average (that must be identical to the previously computed average) and their root-mean square deviation σ_s have been performed. The third measure of broadening comes from considering only the minimum gap for each supercell, then computing the root-mean quare deviation has been computed, and is denoted σ_m. These values are reported in Table 1.

Table 1: Measures of alloy broadening of 16-atom supercells of $Ga_{(1-x)}In_xN$ band gap at different concentration x: average gap supercell root-mean square deviation σ_a, split gap supercell root-mean square deviation σ_s, minimum gap supercell root-mean square deviation σ_m, and the corresponding three flavors of full width at half maximum, namely, FWHM_a (from σ_a), FWHM_s (from σ_s) and FWHM_m (from σ_m). The FWHM values include the effect of thermal broadening of 1.8 kT at room temperature. Experimental values for the FWHM are between 0.08 eV and 0.21 eV.

x	σ_a (eV)	σ_s (eV)	σ_m (eV)	FWHM_a (eV)	FWHM_s (eV)	FWHM_m (eV)
0.25	0.0419	0.0872	0.1044	0.1091	0.2105	0.2502
0.375	0.0514	0.0994	0.0450	0.1297	0.2386	0.1158
0.5	0.0610	0.1350	0.0732	0.1510	0.3213	0.1785
0.625	0.0313	0.0686	0.0290	0.0871	0.1681	0.0827
0.75	0.0167	0.0334	0.0412	0.0609	0.0914	0.1076

Then, they were combined to the natural thermal broadening of 1.8 kT (*i.e.*, 0.0465 eV at room temperature) to estimate the spectral width at room temperature. The combination is not a simple addition, but square root of the sum of the squared values. Moreover there is a factor of 2 log2 $\approx$ 2.355 between a root mean square deviation and a full width at half maximum (FWHM). The values for the three corresponding full width at half maximum FWHM_a (from σ_a), FWHM_s (from σ_s) and FWHM_m (from σ_m) are also reported in Table 1.

The values for FWHM are comparable to the experimental data[32–36] that are in the range between 3kT and 8kT (that is, between 0.08 eV and 0.21 eV), with a tendency for FWHM_a to be in the lower range of experimental values, σ_s to exceeds the experimental data, and σ_m to cover more than the experimental range. A more sophisticated analysis of the origin of the FWHM than these three indicators might be interesting. Because we rely on 16-atom supercells, with two to five models for each concentration only, one should not expect to be quantitatively predictive anyhow. On the contrary, relying on much larger supercells cannot be done based on the exhaustive set of configurations, but should rely on a large statistical sampling of such cells, which goes beyond the present study. We note, however, that the local statistical fluctuations in 16-atom cells are sufficient to obtain the right order of magnitude for the alloy broadening. Actually, none of the previous studies had included such computation of FWHM.

If we focus on the x=0.5 case, the five different crystal structures for $x = 0.5$ (Fig. 1(f, g, h, i and j)) deliver five different band gap values. Among them, one note that the presence of a mono-atomic specie plane within the crystal structure (see Fig. 1(a, c and f)) generates the highest volume per atom characteristics with respect to the other geometrical configurations for each x. This means that the presence of mono-atomic specie plane gives the lowest band gap, with the highest b (see Supporting Information Tab.9-12).

Conclusion

In our study, after having analyzed the InN band gap, and shown that the TB09 approach was sufficiently predictive with respect to reference G_0W_0@TB09 calculations, we have estimated an average bowing parameter b equal to 1.39 eV based on the examination of band gaps in all atomic configurations of a 16-atom supercell. The value of b has been analyzed in terms of bowing of the band gap from the lattice parameter change at fixed concentration (which accounts for about two fifth of the bowing, although the volume change with respect to

concentration is linear) and bowing of the band gap due to atomic configuration distribution at fixed volume. The broadening of the emission spectrum has also been analyzed, showing that the combination of thermal and alloy broadenings, the latter computed from the set of all possible 16-atom supercells, gives qualitative agreement with the experimental broadening. Such analysis had not been performed in earlier theoretical studies.

This investigation has shown more or less the same bowing for In- and Ga-rich $Ga_{(1-x)}In_{(x)}N$ alloys (see Fig. 4). It was seen that the geometrical arrangement with highest volume per atom will linearly reduce the band gap, but will increase the bowing. Such bowing reduction can be obtained choosing the geometrical arrangement at fixed x which avoid mono-atomic specie layer within unit cell. Thus, the synthesis of beam epitaxy films[21,22,25,40] should be avoided, because it is responsible of largest b in $Ga_{(1-x)}In_{(x)}N$ alloys. Such kind of crystal growth should be responsible of mono-atomic specie layer within unit cell. $Ga_{(1-x)}In_{(x)}N$ alloys with the lowest bowing parameter b can be fruitfully used to model LEDs for several colours in the all range of visible spectra.

Acknowledgement

The authors would like to thank the Siberian Super-Computer Center of the Siberian Branch of the Russian Academy of Sciences for computational resources. This work was supported by Russian state assignment to ISSCM SB RAS (project no. FWUS-2021-0005).

Supporting Information Available

References

(1) Zhuk, S.; Kistanov, A. A.; Boehme, S. C.; Ott, N.; Stiefel, M.; Kovalenko, M. V.; Siol, S. Synthesis of a new ternary nitride semiconductor – Zn_2VN_3: A combinatorial exploration of the Zn-V-N phase space. 2021.

(2) Schulz, H.; Thiemann, K. H. Crystal structure refinement of AlN and GaN. *Solid State Commun.* **1977**, *23*, 815.

(3) Wright, A. F.; Nelson, J. S. Consistent structural properties for AlN, GaN, and InN. *Phys. Rev. B* **1995**, *51*, 7866.

(4) Gorczyca, I.; Christensen, N. E. Band structure and high-pressure phase transition in GaN, AlN, InN and BN. *Physica B* **1993**, *185*, 410.

(5) Greenaway, A. L.; Melamed, C. L.; Tellekamp, M.; Woods-Robinson, R.; Toberer, E. S.; Neilson, J. R.; Tamboli, A. C. Ternary Nitride Materials: Fundamentals and Emerging Device Applications. *arXiv:cond-mat.mtrl-sci* **2020**, *v1*, 2010.08058.

(6) Dingle, R.; Sell, D. D.; Stokowski, S. E.; Ilegems, M. Absorption, Reflectance, and Luminescence of GaN Epitaxial Layers. *Appl. Phys. Lett.* **1971**, *4*, 1211.

(7) Landolt-Börnstein, *Numerical Data and Functional Relationships in Science and Technology, Tables Vol. III/17a*; Hellwege Springer, New York, 1982.

(8) Gorczyca, I.; Łepkowski, S. P.; Suski, T.; Christensen, N. E.; Svane, A. Influence of indium clustering on the band structure of semiconducting ternary and quaternary nitride alloys. *Phys. Rev. B* **2009**, *80*, 075202.

(9) Orton, J. W. Effect of strain on GaN exciton spectra. *Semicond. Sci. Technol.* **1996**, *11*, 1026.

(10) Chen, G. D.; Smith, M.; Lin, J. Y.; Jiang, H. X.; Wei, S. H.; Khan, M. A.; Sun, C. J. Fundamental optical transitions in GaN. *Appl. Phys. Lett.* **1996**, *68*, 2784.

(11) Edwards, N. V., et al. Band parameters for nitrogen-containing semiconductors. *Appl. Phys. Lett.* **1997**, *70*, 2001.

(12) Gorczyca, I.; Suski, T.; Christensen, N. E.; Svane, A. Band gap bowing in quaternary nitride semiconducting alloys. *Applied Physics Letters* **2011**, *98*, 241905.

(13) César, M.; Ke, Y.; Ji, W.; Guo, H.; Mi, Z. Band gap of $In_xGa_{1-x}N$: A first principles analysis. *Applied Physics Letters* **2011**, *98*, 202107.

(14) Cui, Y.; Lee, S.; Freysoldt, C.; Neugebauer, J. Role of biaxial strain and microscopic ordering for structural and electronic properties $In_{(x)}Ga_{(1-x)}N$. *Phys. Rev. B* **2015**, *92*, 085204.

(15) Pugh, S. K.; Dugdale, D. J.; Brand, S.; Abram, R. A. Band-gap and k.p. parameters for GaAlN and GaInN alloys. *J. Appl. Phys.* **1999**, *86*, 3768.

(16) McCluskey, M. D.; Van de Walle, C. G.; Master, C. P.; Romano, L. T.; Johnson, N. M. Large band gap bowing of alloys $In_{(x)}Ga_{(1-x)}N$. *Appl. Phys. Lett.* **1998**, *72*, 2725.

(17) McCluskey, M. D.; Van de Walle, C. G.; Romano, L. T.; Krusor, B. S.; Johnson, N. M. Effect of composition on the band gap of strained $In_{(x)}Ga_{(1-x)}N$ alloys. *Journal of Applied Physics* **2003**, *93*, 4340.

(18) Bergmann, M. J.; Casey, H. C. Optical-field calculations for lossy multiple-layer $Al_{(x)}Ga_{(1-x)}/In_{(x)}Ga_{(1-x)}N$ laser diodes. *Journal of Applied Physics* **1998**, *84*, 1196.

(19) Martin, R. W.; Edwards, P. R.; Hernandez, S.; Wang, K.; Fernandez-Torrente, I.; Kurouchi, M.; Nanishi, Y.; O'Donnell, K. P. The composition dependence of the optical properties of InN-rich InGaN grown by MBE. *MRS Online Proceedings Library* **2004**, *831*, 479–484.

(20) Stepanov, S.; Wang, W. N.; Yavich, B. S.; Bougrov, V.; Rebane, Y. T.; Shreter, Y. G. Influence of Poisson's ratio uncertainty on calculations of the bowing parameter for strained InGaN layers. *Materials Research Society Internet Journal of Nitride Semiconductor Research* **2001**, *6*, 6.

(21) Wu, J.; Walukiewicz, W.; Shan, W.; Yu, K. M.; Ager III, J. W.; Haller, E. E.; Lu, H.;

Schaff, W. J. Effects of the narrow band gap on the properties of InN. *Phys. Rev. B* **2002**, *66*, 201403.

(22) Wu, J.; Walukiewicz, W.; Yu, K. M.; Ager III, J. W.; Haller, E. E.; Lu, H.; Schaff, W. J. Small bandgap bowing in $In_{(1-x)}Ga_xN$ alloys. *Appl. Phys. Lett.* **2002**, *80*, 3967.

(23) Pereira, S.; Correia, M. R.; Monteiro, T.; Pereira, E.; Alves, E.; Sequeira, A. D.; Franco, N. Structural and optical properties of InGaN/ GaN layers close to the critical layer thickness. *Appl. Phys. Lett.* **2001**, *78*, 2137.

(24) Shan, W.; Walukiewicz, W.; Haller, E. E.; Little, B. D.; Song, J. J.; McCluskey, M. D.; Johnson, N. M.; Feng, Z. C.; Schurman, M.; Stall, R. A. Optical properties of $In_{(x)}Ga_{(1-x)}N$ alloys grown by metalorganic chemical vapor deposition. *J. App. Phys.* **1998**, *84*, 4452.

(25) Davydov, V. Y.; Klochikhin, A. A.; Seisyan, R. P.; Emtsev, V. V.; Ivanov, S. V.; Bechstedt, F.; Furthmüller, J.; Harima, H.; Mudryi, A.; Aderhold, J.; Semchinova, O.; Graul, J. Absorption and Emission of Hexagonal InN. Evidence of Narrow Fundamental Band Gap. *Phys. Status Solidi B* **2002**, *229*, R3.

(26) Takeuchi, T.; Takeuchi, H.; Sota, S.; Sakai, H.; Amano, H.; Akasaki, I. Optical Properties of Strained AlGaN and GaInN on GaN. *Jpn. J. Appl. Phys. Part 2* **1997**, *36*, L177.

(27) Scholz, F.; Off, J.; Sohmer, A.; Syganow, V.; Dornen, A.; Ambache, O. MOVPE of GaInN heterostructures and quantum wells. *Journal of Crystal Growth.* **1998**, *189/190*, 8–12.

(28) Wetzel, C.; Takeuchi, T.; Yamaguchi, S.; Katoh, H.; Amano, H.; Akasaki, I. Optical band gap in $Ga_{(1-x)}In_{(x)}N$ ($0 < x < 0.2$) on GaN by photoreflection spectroscopy. *Appl. Phys. Lett.* **1998**, *73*, 1994.

(29) Kim, M.-H.; Cho, J.-K.; Lee, I.-H.; Park, S.-J. Metalorganic Molecular Beam Epitaxy of InGaN Layers and Their Optical Properties. *physica status solidi (a)* **1999**, *176*, 269.

(30) Alam, S. N.; Zubialevich, V. Z.; Ghafary, B.; Parbrook., P. J. Band gap and refractive index estimates of InAlN and related nitrides across their full composition ranges. *Scientific Reports* **2020**, *10*, 16205.

(31) Schygulla, P.; Fuß-Kailuweit, P.; Höhn, O.; Dimroth., F. Determination of the complex refractive index of compound semiconductor alloys for optical device modelling. *J. Phys. D: Appl. Phys.* **2020**, *53*, 495104.

(32) Xi, Y.; Schubert, E. F. Junction–temperature measurement in GaN ultraviolet light-emitting diodes using diode forward voltage method. *Appl. Phys. Lett.* **2004**, *85*, 2163.

(33) Xi, Y.; Crawford, M. H.; Bogart, K. H. A.; Allerman, A. A. Junction and carrier temperature measurements in deep-ultraviolet light-emitting diodes using three different methods. *Appl. Phys. Lett.* **2005**, *86*, 031907.

(34) Schubert, E. F. *Light-Emitting Diodes*; Cambridge University Press, 2006.

(35) Cardona, M.; Thewalt, M. L. W. Isotope effects on the optical spectra of semiconductors. *Review of Modern Physics* **2005**, *77*, 3641.

(36) Nakamura., S. III–V nitride based light-emitting devices. *Solid State Communications.* **1997**, *102*, 237–248.

(37) Sokeland, F.; Rohlfing, M.; Kruger, P.; Pollmann, J. Density functional and quasiparticle band-structure calculations for $Ga_{(x)}Al_{(1-x)}N$ and $Ga_{(x)}In_{(1-x)}N$ alloys. *Phys. Rev. B* **2003**, *68*, 075203.

(38) T. Kuykendall, S. A., P. Ulrich; Yang, P. Complete composition tunability of InGaN nanowires using a combinatorial approach. *Nature Materials* **2007**, *6*, 951–956.

(39) Matsuoka, T.; Okamoto, H.; Nakao, M.; Harima, H.; Kurimoto, E. The composition dependence of the optical properties of InN-rich InGaN grown by MBE. *Appl. Phys. Lett.* **2002**, *81*, 1246.

(40) Inushima, T.; Mamutin, V. V.; Vekshin, V. A.; Ivanov, S. V.; Sakon, T.; Motokawa, M.; Ohoya, S. Physical properties of InN with the band gap energy of 1.1 eV. *J. Crystal Growth* **2001**, *481*, 227.

(41) Scharoch, P.; Winiarski, M. J.; P., P. M. Ab initio study of $In_xGa_{(1-x)}N$ - performance of the alchemical mixing approximation. *Comput. Mater. Sci.* **2014**, *81*, 358–365.

(42) Monemar, B. Fundamental energy gap of GaN from photoluminescence excitation spectra. *Phys. Rev. B* **1974**, *10(2)*, 676–681.

(43) Tansley, T. L.; Foley, C. P. Optical band gap of indium nitride. *Journal of Applied Physics* **1986**, *59(9)*, 3241–3244.

(44) Nakamura., S. InGaN/AlGaN blue light emitting diodes. *Journal of Vacuum Science and Technology A.* **1995**, *13*, 705.

(45) Caetano, C.; Teles, L. K.; Marques, M.; Jr., A. D. P.; Ferreira., L. G. Phase stability, chemical bonds, and gap bowing of $In_{(x)}Ga_{(1-x)}N$ alloys: Comparison between cubic and wurtzite structures. *Phys. Rev. B* **2006**, *74*, 045215.

(46) Pelà, R. R.; Caetano, C.; Marques, M.; Ferreira, L. G.; Furthmüller, J.; Teles., L. K. The composition dependence of the optical properties of InN-rich InGaN grown by MBE. *Appl. Phys. Lett.* **2011**, *98*, 151907.

(47) Heyd, J.; Scuseria, G. E.; Ernzerhof, M. Hybrid functionals based on a screened Coulomb potential. *J. Chem. Phys.* **2003**, *118*, 8207.

(48) Moses, P. G.; Van de Walle, C. G. Band bowing and band alignment in InGaN alloys. *App. Phys. Lett.* **2010**, *96*, 021908.

(49) Moses, P. G.; Miao, M.; Yan, Q.; Van de Walle, C. G. Hybrid functional investigations of band gaps and alignments in GaN, InN and InGaN. *J. Chem. Phys.* **2011**, *134*, 084703.

(50) Yan, Q.; Rinke, P.; A., J.; Scheffler, M.; Van de Walle, C. G. Effects of strain on the band structure of group-III nitrides. *Phys. Rev. B* **2014**, *90*, 125118.

(51) Martin, R. M.; Reining, L.; Ceperley, D. *Interacting electrons*; Cambridge University Press, 2016.

(52) Hedin, L. New Method for Calculating the One-Particle Green's Function with Application to the Electron-Gas Problem. *Phys. Rev. A* **1965**, *139*, 795.

(53) Perdew, J. P.; Ernzerhof, M.; Burke, K. Rationale for mixing exact exchange with density functional approximations. *J. Chem. Phys.* **1996**, *105*, 9982.

(54) Shishkin, M.; Kresse, G. Self-consistent *GW* calculations for semiconductors and insulators. *Phys. Rev. B* **2007**, *5*, 235102.

(55) van Setten, M. J.; Giantomassi, M.; X. Gonze, G. R.; Hautier, G. Automation methodologies and large-scale validation for *GW*: Towards high-throughput *GW* calculations. *Physical Review B* **2017**, *96*, 155207.

(56) Tran, F.; Blaha, P. Accurate Band Gaps of Semiconductors and Insulators with a Semilocal Exchange-Correlation Potential. *Phys. Rev. Lett.* **2009**, *102*, 226401.

(57) Waroquiers, D.; Lherbier, A.; Miglio, A.; Stankovski, M.; Poncé, S.; Oliveira, M. J. T.; Giantomassi, M.; Rignanese, G.-M.; Gonze, X. Band widths and gaps from the Tran-Blaha functional: Comparison with many-body perturbation theory. *Phys. Rev. B* **2013**, *87*, 075121.

(58) Poncé, S.; Gillet, Y.; Laflamme Janssen, J.; Marini, A.; Verstraete, M.; Gonze, X.

Temperature dependence of the electronic structure of semiconductors and insulators. *The Journal of Chemical Physics* **2015**, *143*, 102813.

(59) Miglio, A.; Brousseau-Couture, V.; Godbout, E.; Antonius, G.; Chan, Y.-H.; Louie, S. G.; Côté, M.; Giantomassi, M.; Gonze, X. Predominance of non-adiabatic effects in zero-point renormalization of the electronic band gap. *npj Computational Materials* **2020**, *6*, 167.

(60) Svane, A.; Christensen, N. E.; Gorczyca, I.; van Schilfgaarde, M.; Chantis, A. N.; Kotani, T. Quasiparticle self-consistent GW theory of III-V nitride semiconductors: Bands, gap bowing, and effective masses. *Phys. Rev. B* **2010**, *82*, 115102.

(61) Momma, K.; Izumi, F. VESTA 3 for three-dimensional visualization of crystal, volumetric and morphology data. *J. Appl. Crystallogr.* **2011**, *44*, 1272.

(62) Broyden, C. G. The Convergence of a Class of Double-Rank Minimization Algorithms 1. General Considerations. *IMA J. Appl. Math.* **1970**, *6 (1)*, 76–90.

(63) Goldfarb, D. A Family of Variable-Metric Methods Derived by Variational Means. *Math. Comp.* **1970**, *24 (109)*, 23–26.

(64) Shanno, D. F. Conditioning of Quasi-Newton Methods for Function Minimization. *Math. Comp.* **1970**, *24 (111)*, 647–656.

(65) Steihaug, T. *Practical Methods of Optimization Volume 1: Unconstrained Optimization*; Wiley, New York, 1980.

(66) Jollet, F.; Torrent, M.; Holzwarth, N. A. Generation of Projector Augmented-Wave atomic data: A 71 element validated table in the XML format. *Computer Physics Communications* **2013**, *185*, 1246.

(67) Hartwigsen, C.; Goedecker, S.; Hutter, J. Relativistic separable dual-space Gaussian pseudopotentials from H to Rn. *Phys. Rev. B* **1998**, *58*, 3641.

(68) Klimes, J.; Kaltak, M.; Kresse, G. Predictive GW calculations using plane waves and pseudopotentials. *Phys. Rev. B* **2014**, *90*, 075125.

(69) Gonze, X. et al. Recent developments in the ABINIT software package. *Computer Physics Communications* **2016**, *205*, 106–131.

(70) Gonze, X. et al. The Abinit project: Impact, environment and recent developments. *Computer Physics Communications* **2020**, *248*, 107042.

(71) Romero, A. H. et al. ABINIT: Overview, and focus on selected capabilities. *J. Chem. Phys.* **2020**, *152*, 124102.